

1 Sustained intensification of the Aleutian Low induces weak  
2 tropical Pacific sea surface warming

3  
4 William J. Dow<sup>1</sup>, Christine M. McKenna<sup>1</sup>, Manoj M. Joshi<sup>2</sup>, Adam T. Blaker<sup>3</sup>, Richard Rigby<sup>1</sup>,  
5 Amanda C. Maycock<sup>1</sup>

6  
7 <sup>1</sup>School of Earth and Environment, University of Leeds, Leeds, UK

8 <sup>2</sup>Climatic Research Unit, School of Environmental Sciences, University of East Anglia, Norwich,  
9 UK

10 <sup>3</sup>National Oceanography Centre, Southampton, UK

11

12

13

14 **Abstract**

15

16 It has been proposed that externally forced trends in the Aleutian Low can induce a basin-wide  
17 Pacific SST response that projects onto the pattern of the Pacific Decadal Oscillation (PDO). To  
18 investigate this hypothesis, we apply local atmospheric nudging in an intermediate complexity  
19 climate model to isolate the effects of an intensified winter Aleutian Low sustained over several  
20 decades. An intensification of the Aleutian Low produces a basin-wide SST response with a  
21 similar pattern to the model's internally-generated PDO. The amplitude of the SST response in  
22 the North Pacific is comparable to the PDO, but in the tropics and southern subtropics the  
23 anomalies induced by the imposed Aleutian Low anomaly are a factor of 3 weaker than for the  
24 internally-generated PDO. The tropical Pacific warming peaks in boreal spring, though anomalies  
25 persist year-round. A heat budget analysis shows the northern subtropical Pacific SST response  
26 is predominantly driven by anomalous surface turbulent heat fluxes in boreal winter, while in the  
27 equatorial Pacific the response is mainly due to meridional heat advection in boreal spring. The  
28 propagation of anomalies from the extratropics to the tropics can be explained by the seasonal  
29 footprinting mechanism, involving the wind-evaporation-SST feedback. The results show that low  
30 frequency variability and trends in the Aleutian Low could contribute to basin-wide anomalous  
31 Pacific SST, but the magnitude of the effect in the tropical Pacific, even for the extreme Aleutian  
32 Low forcing applied here, is small. Therefore, external forcing of the Aleutian Low is unlikely to  
33 account for observed decadal SST trends in the tropical Pacific in the late 20th and early-21st  
34 centuries.

35  
36  
37  
38  
39  
40  
41  
42  
43  
44  
45  
46  
47  
48

Key points (140 chars)

1. A sustained intensification of the winter Aleutian Low produces weak warming in the tropical Pacific that peaks in spring.
2. Changes to surface heat fluxes (subtropics) during boreal winter and meridional advection (equatorial) during boreal spring in the upper ocean drive the SST warming.
3. A combination of the seasonal footprint mechanism and wind-evaporation-SST mechanism generate the surface climate anomalies in the tropical Pacific.

## 49 1. Introduction

50

51 The Aleutian Low has a well-known role in determining the North Pacific component of the Pacific  
52 Decadal Oscillation (PDO) (e.g. Schneider and Cornuelle, 2005; Zhang et al., 2018; Hu and Guan,  
53 2018; Sun and Wang, 2006; Newman et al. 2016). Fluctuations in Aleutian Low intensity affect  
54 the North Pacific subpolar gyre (Pickart et al. 2008), upper ocean temperatures (e.g. Latif and  
55 Barnett, 1996) and sea surface height (Nagano and Wakita, 2019) through anomalous thermal  
56 forcing and wind stress. Oceanic Rossby waves initiated by Aleutian Low variability can propagate  
57 westward and cause lagged signals in the Kuroshio-Oshashio Extension (KOE) region (e.g.,  
58 Kwon and Deser, 2007).

59

60 The traditional paradigm for the PDO describes the integrated effect of mid-latitude stochastic  
61 variability, which induces SST anomalies through turbulent heat flux and wind stress curl  
62 anomalies, and driving from tropical processes (ENSO variability) via excitation of Rossby wave  
63 trains and tropical-extratropical teleconnections (Newman et al. 2016; Zhao et al. 2021; Vimont.  
64 2005; Knutson and Manabe 1998; Jin 2001). We note that recent definitions separate low  
65 frequency PDO variability and show this is predominantly associated with stochastic extratropical  
66 atmospheric variability (i.e. the Aleutian Low) (Wills et al., 2018, 2019). However, decadal  
67 changes in the Aleutian Low may arise via other mechanisms including Arctic sea ice trends  
68 (Simon et al. 2021; Deser et al. 2016), stratospheric polar vortex variability (Richter et al., 2015),  
69 or as a local response to external forcings (Smith et al. 2016; Dow et al. 2021; Dittus et al. 2021;  
70 Klavans et al. submitted). It has been proposed that observed shifts in the PDO in the late 20th  
71 and early 21st centuries were driven by anthropogenic forcing of the Aleutian Low, which was  
72 then communicated to a basin-wide PDO signal (Smith et al. 2016; Klavans et al. submitted; Gan  
73 et al. 2017). However, the mechanisms via which North Pacific anomalies linked to decadal  
74 Aleutian Low changes may be communicated into a basin-wide SST response including the  
75 tropics, and whether the amplitude of such a response matches observed variations, remain  
76 unclear.

77

78 Several studies have investigated the North Pacific influence on the tropics using surface flux  
79 restoring in a model (Alexander et al. 2010; Sun and Okumura 2019; Liu et al. 2021). Alexander  
80 et al. (2010) and Sun and Okumura (2019) imposed surface flux anomalies derived from the North  
81 Pacific Oscillation (NPO) - the anomalous North Pacific pattern projecting onto the second EOF  
82 of low frequency tropical Pacific SST variability. They showed that surface forcing associated with  
83 the NPO can affect decadal variability in the tropics. The proposed mechanism for communicating

84 extratropical surface anomalies to the tropics is the seasonal footprinting mechanism (SFM)  
85 (Alexander et al. 2010; Sun and Okumura 2019; Amaya et al. 2019, Liu et al. 2021). Atmospheric  
86 circulation anomalies driven by the subtropical portion of the high latitude SST footprint modulate  
87 tropical SSTs through coupled atmosphere-ocean processes, leading to anomalies that persist  
88 through boreal spring-summer. However, the amplitude of the effect on tropical Pacific SSTs from  
89 the North Pacific has been suggested to be quite weak on decadal timescales (Alexander et al.  
90 2010; Sun and Okumura 2019; Liguori and Di Lorenzo 2019). Moreover, the studies did not  
91 directly isolate driving by the Aleutian Low, which has been highlighted in studies arguing a role  
92 for anthropogenic forcing of recent observed PDO variability (Smith et al. 2016; Klavans et al.  
93 submitted).

94  
95 In this study, we aim to better understand the role of long-term changes in the Aleutian Low in  
96 governing the multi-annual behaviour of tropical Pacific SSTs. We perform an ensemble of  
97 atmospheric nudging simulations in an intermediate complexity coupled climate model to isolate  
98 the effect of a sustained anomaly in the Aleutian Low. The response to this regional perturbation  
99 is compared to the internally-generated low frequency Pacific variability in a free running  
100 simulation. The manuscript is structured as follows: section 2 describes the methodology and  
101 details of the model used. Section 3 compares the results of the nudging simulations with the free  
102 running simulation. Discussion of the results is provided in section 4 and conclusions in section  
103 5.

104  
105

## 106 **2. Data and Methods**

107  
108  
109

### 2.1 FORTE 2.0

110 Simulations were performed using FORTE2.0, an intermediate complexity coupled Atmosphere-  
111 Ocean General Circulation Model (AOGCM) (Blaker et al., 2021). The atmospheric model IGCM4  
112 (Intermediate General Circulation Model 4) (Joshi et al., 2015) uses a truncated series of spherical  
113 harmonics run at T42 resolution with 20  $\Sigma$ -levels to a height of  $\Sigma = 0.05$ . IGCM4 is coupled to the  
114 MOMA (Modular Ocean Model – Array) (Webb, 1996) ocean model run at  $2^\circ \times 2^\circ$  resolution with  
115 15 vertical levels. The two components are coupled once per day using OASIS version 2.3 (Terray  
116 et al., 1999) and PVM version 3.4.6 (Parallel Virtual Machine). As described in Blaker et al. (2021),  
117 between  $5^\circ$  N/S and the equator the horizontal ocean diffusion increases by a factor of 20 to

118 balance equatorial upwelling and parameterise the eddy heat convergence. For more details on  
 119 the model see Blaker et al. (2021). The model simulates multi-decadal SST variability in the  
 120 Pacific with a similar pattern to that seen in observations but a weaker amplitude by around a  
 121 factor of 4 to 5 (Figure S1).

122

## 123 **2.2 Grid-point nudging method**

124

125 Atmospheric nudging has been used to investigate climate and weather relationships between  
 126 remote phenomena (e.g. Martin et al., 2021; Knight et al., 2017; Watson et al., 2016). A nudging  
 127 code was added to ICGM4. Nudging was performed by adding tendencies to horizontal winds,  
 128 temperature and surface pressure. The nudging code is publicly available at  
 129 (<https://github.com/NOC-MSM/FORTE2.0>).

130 The nudging configuration is similar to that in Watson et al. (2016), with two additional terms to  
 131 account for vertical (z) and temporal (t) variation in the nudging strength:

$$132 \quad \delta x(\lambda, \phi, z, t) = -\gamma(\lambda, \phi, z, t) (x(\lambda, \phi, z, t) - x_{ref}(\lambda, \phi, z, t)) / \tau, \quad (\text{Eqn 1})$$

133 where  $x$  is the variable being relaxed as a function of longitude ( $\lambda$ ), latitude ( $\phi$ ), vertical coordinate ( $z$ ), and time ( $t$ ).  $x_{ref}$  is the reference  
 134 state, and  $\gamma$  is the nudging strength (set to 6hr). The spatial extent of the nudging was tested  
 135 extensively to avoid any shock at the boundaries and spurious effects of nudging near polar  
 136 regions. The regional extent was determined as:

$$137 \quad \gamma(\phi, \lambda) = f(\phi, \phi_1, \phi_2) f(\lambda, \lambda_1, \lambda_2), \quad (\text{Eqn 2})$$

138 where

$$139 \quad f(\phi, \phi_1, \phi_2) = [1/(1 + e^{-(\phi-\phi_1)/\delta_1})][1 - 1/(1 + e^{-(\phi-\phi_2)/\delta_2})] \quad (\text{Eqn 3})$$

140 and

$$141 \quad f(\lambda, \lambda_1, \lambda_2) = [1/(1 + e^{-(\lambda-\lambda_1)/\delta_1})][1 - 1/(1 + e^{-(\lambda-\lambda_2)/\delta_2})] \quad (\text{Eqn 4}).$$

142

143  $\Phi_1 = 30^\circ\text{N}$  and  $\Phi_2 = 65^\circ\text{N}$  represent the southern and northern limits of the nudging region and  $\lambda_1$   
 144  $= 160^\circ\text{E}$  and  $\lambda_2 = 140^\circ\text{W}$  are the western and eastern limits of the nudging region. The horizontal

145 limits follow the commonly defined North Pacific Index (NPI) (Trenberth and Hurrell, 1994) as a  
146 proxy for the region encompassed by the Aleutian Low.

147 The temporal and nudging variations are determined as:

148 
$$f(z) = a \cdot \exp(bz) \quad (\text{Eqn 5})$$

149 
$$f(t) = \left( \frac{1}{\exp\left(-0.5 \cdot \left(\frac{d^2}{\beta^2}\right)^{2\mu}\right)} \right) \quad (\text{Eqn 6})$$

150 The strength of the tropospheric nudging is set to 1 (constant  $a$ , Equation 5) at  $\Sigma = 0.96$  (lowest  
151 atmospheric level), decreasing exponentially to 0 at  $\Sigma = 0.05$  (tropopause) (Equation 5). Nudging  
152 is applied during the extended boreal winter season (NDJFM) peaking on 15 January, with a  
153 Gaussian function in time to increase the nudging strength from 0 to 1 between 1 to 30 November  
154 and a reverse ramp-down during March. Term  $d$  (Equation 6) is the day within the nudging period,  
155  $\beta$  is a constant set to 1.2,  $\mu$  is a constant set to 2. The spatio-temporal forms of the nudging  
156 coefficients are shown in Figure S2.

157 The strong Aleutian Low state is taken from a 100 year long control run (CONTROL) based on a  
158 winter month with an NPI anomaly of  $-3.02\sigma$  ( $-10.76$  hPa), where  $\sigma$  is the standard deviation  
159 calculated over all winter months in CONTROL (Figure S3). Therefore, the target state represents  
160 an extreme intense Aleutian Low state as simulated in FORTE2.0. Comparing with ERA5  
161 reanalysis data from 1979-2020, the most intense winter month has an NPI anomaly of  $-3.56\sigma$  ( $-$   
162  $18.13$  hPa). The imposed atmospheric forcing is therefore weaker than if an equivalent  
163 experiment was conducted using reanalysis data.  $x_{ref}$  comprises the anomaly of the chosen  
164 month added to the daily climatology. A 50 member NUDGED ensemble was generated using  
165 initial conditions drawn from each January 1<sup>st</sup> of the final 50 years of CONTROL. Each member  
166 is integrated for 30 years with nudging commencing on 1 November of the first year and repeating  
167 each winter of the simulation. Unless otherwise stated, the analysis shows ensemble mean  
168 anomalies in the NUDGED simulation compared to the long-term climatology of CONTROL.  
169 Statistical significance is defined by comparing the responses to the magnitude of simulated  
170 unforced decadal variability. At each grid point, overlapping 15-year mean anomalies are  
171 calculated from CONTROL. A 15-year time window was chosen to adequately capture decadal  
172 internal variability. The standard deviation of the mean anomalies from CONTROL was multiplied  
173 by square root of 2 to account for the fact that the variability of a difference in means is of interest.

174 This estimates the variation of the difference in standard deviation between two independent  
 175 averages, which have the same variance, that would be expected due to internal variability. The  
 176 median value of the standard deviations is used and we show 95% significance as where the  
 177 response value lies outside of the bounds 1.96 times the median standard deviation. This is similar  
 178 to the method used in IPCC AR5 (2013).

179

180

### 181 **2.3 Mixed Layer Heat Budget Analysis**

182 The heat budget of the upper 30m of the ocean (representing the mixed layer) is analysed for the  
 183 regions shown by the boxes in Figure 1, where the temperature tendency is given by:

$$184 \quad dT/dt = ADV + DIFF_{\text{vert}} + DIFF_{\text{horiz}} + CONV \text{ (Eqn. 7).}$$

185 Daily tendencies due to advection (ADV), vertical and horizontal diffusion ( $DIFF_{\text{vert}}$  and  $DIFF_{\text{horiz}}$ )  
 186 and convection (CONV) are output from the model. Further granularity in the heat budget terms  
 187 (e.g. turbulent fluxes) was not possible due to the limited availability of diagnostics from the  
 188 model. Vertical diffusion represents the contribution to the mixed layer heat budget from surface  
 189 turbulent and radiative fluxes. ADV is composed of zonal, meridional and vertical components:

$$190 \quad ADV = u \frac{\delta T}{\delta x} + v \frac{\delta T}{\delta y} + w \frac{\delta T}{\delta z}$$

191 (Eqn. 8)

192 where u, v and w are the zonal, meridional and vertical components of the ocean velocity and  
 193  $dT/dx$  represents the local zonal gradient of temperature. We linearize the meridional advection  
 194 term to investigate the relative roles of changes to ocean current velocity and temperature  
 195 gradient as follows:

$$196 \quad \left( v \frac{\delta T}{\delta y} \right)' = v' \frac{\delta T_0}{\delta y} + v_0 \left( \frac{\delta T}{\delta y} \right)' + v' \left( \frac{\delta T}{\delta y} \right)' \text{ (Eqn. 9)}$$

197 where the subscript 0 denotes CONTROL values and primes denote anomalies in NUDGED.

### 198 **2.4 PDO Index**

199 The PDO index is calculated as the first EOF of monthly SST anomalies, calculated as deviations  
200 from the climatological seasonal cycle, over the region 20-65°N, 120-260°E (Mantua et al. 1997).  
201 Before calculating the leading EOF, the temperature anomalies are weighted by the square-root  
202 of the cosine of latitude to account for the decrease in area towards the pole. The monthly principal  
203 component, corresponding to the PDO index, is normalised by the standard deviation to give it  
204 unit variance. The pattern of temperature anomalies that covaries with the PDO is found by  
205 linearly regressing the time series of the monthly mean temperature anomalies onto the monthly  
206 PDO index (Figure 1b). Here we define the PDO using the common index based on the leading  
207 EOF of North Pacific SST variability. Wills et al. (2019) showed that the tropical Pacific SST  
208 anomalies associated with this index are predominantly related to high frequency (e.g., ENSO)  
209 SST variability, while the extratropical part is related to turbulent heat flux and wind stress  
210 anomalies associated with intrinsic Aleutian Low variability. The discrepancy between the  
211 modelled and observed SST anomalies associated with the PDO index in Figure S1 could be due  
212 to the slightly weaker than observed ENSO amplitude in the model by around 33% (Figure S4)  
213 (see also Blaker et al., 2021).

### 214 **3. Results**

215

#### 216 *3.1 Surface temperature response*

217 Figure 1a shows annual mean surface temperature anomalies in NUDGED expressed as a  
218 change per standard deviation ( $\sigma$ ) of the PDO index. A horse-shoe pattern of anomalous  
219 temperature extends across the North Pacific, comprising warming in the north and eastern  
220 Pacific and along the west coast of North America and cooling in the western North Pacific/KOE  
221 region. The strongest warming (0.2-0.3 K/ $\sigma$ ) is seen over the North Pacific and western North  
222 America. There is weaker (0.02-0.04 K/ $\sigma$ ) but statistically significant warming in the eastern and  
223 central equatorial Pacific. Across the Pacific ocean, the pattern of temperature anomalies in  
224 NUDGED closely resembles unforced multidecadal Pacific variability in CONTROL (Figure 1b),  
225 with a pattern correlation coefficient of 0.53. Therefore, a sustained increase in Aleutian Low  
226 strength forces a basin-wide SST response which resembles that associated with internally-  
227 generated coupled variability in CONTROL. However, there are clear differences in the sign of  
228 the anomaly outside the North Pacific basin and nudging region, such as over north-eastern  
229 Siberia and south-central USA. Furthermore, while the extratropical SST anomalies are  
230 somewhat larger in NUDGED, particularly in the subpolar gyre, the tropical Pacific signal is  
231 substantially weaker by a factor of  $\sim 3$ . This indicates that atmospheric forcing by the Aleutian Low  
232 alone is not sufficient to generate a basin-wide SST response that is consistent with the intrinsic



233 variability of the model. Note the Aleutian Low state in  $x_{\text{ref}}$  is extreme ( $-3\sigma$ ), meaning a more  
234 realistic amplitude for sustained Aleutian Low intensification can be expected to induce a weaker  
235 response.

236 The seasonality of the surface temperature anomalies in NUDGED is shown in Figure 2 separated  
237 for years 1-2, years 3-4 and years 5-30. The initial response to the intensified Aleutian Low is a  
238 warming in the subpolar gyre in boreal autumn (SON). This amplifies in DJF during the peak of  
239 the nudging period, where a tongue of warming extends into the subtropical North Pacific. This  
240 pattern persists into MAM after nudging ceases but is also accompanied by warming in the  
241 eastern tropical Pacific. By JJA, the tropical and subtropical temperature changes have weakened  
242 leaving residual warming in the subpolar gyre that persists into the following winter. The  
243 temperature anomalies over land quickly dissipate due to the low specific heat capacity. A similar  
244 seasonal evolution occurs in years 3-4, but the tropical warm anomaly emerges earlier in DJF  
245 and extends further westward at its peak in MAM. The anomalies in years 5-30 show a similar  
246 spatiotemporal pattern to the first 4 years, suggesting the mechanisms by which the anomalies  
247 manifest do not evolve strongly when the signals are maintained over multi-year timescales. Small  
248 differences between years 1-4 and 5-30 are the extent of the robust signal in the tropical Pacific;  
249 there is a small reduction in the amplitude of the tropical warming in JJA and no significant western  
250 tropical Pacific warming in MAM for years 5-30. The signal of peak tropical warming in MAM in  
251 NUDGED qualitatively agrees with observed low frequency Pacific variability (Figure S1), though  
252 we note that FORTE2.0 shows a narrower band of tropical warming compared to observations.  
253 Furthermore, the weak footprint of modelled PDO variability in the equatorial Pacific (Fig. S1) is  
254 consistent with a notion that Aleutian Low driven SST variability in the extra-tropics has little  
255 influence on tropical variability (Wills et al., 2019; Zhao et 2021).

256

### 257 *3.2 Mixed layer heat budget*

258 The mixed layer heat budget in the subtropical North Pacific and Niño 3.4 regions shows different  
259 annual cycles in the anomalous temperature tendencies (Figure 3 a,b). The largest anomalous  
260 surface temperature tendency in the subtropical North Pacific occurs during the nudging period  
261 (DJF), whereas the peak warming tendency in the Niño3.4 region occurs in February-April. In the  
262 subtropics in winter, warming from vertical diffusion is offset by meridional advection. In contrast  
263 in the Niño 3.4 region, anomalous meridional advection contributes to a warming tendency year-  
264 round, with the maximum ( $\sim 0.3$  K/month) in MAM. This warming is partly offset by anomalous  
265 vertical diffusion and convection. Meridional advection therefore contributes to cooling in the  
266 subtropical North Pacific but causes warming in the Niño 3.4 region.

267

268 The anomalous meridional advection in the subtropical North Pacific is dominated by the change  
269 in meridional velocity, whilst in the Niño3.4 region the change in meridional temperature gradient  
270 is the largest contributor throughout most of the year (apart from Sept-Dec). The enhanced  
271 warming tendency from Feb-June in the Niño3.4 region is driven by changes in meridional  
272 velocity. The difference in contributing terms implies different mechanisms governing the  
273 changing mixed layer temperatures in the two regions.

274

275 The net surface heat flux anomalies in NUDGED are shown in Figure 4(a-d). There are positive  
276 net surface heat flux anomalies across the North Pacific and within a SW-NE oriented band in the  
277 subtropical North Pacific. The largest heat flux anomalies occur during DJF, with values in excess  
278 of  $4 \text{ W m}^{-2}/\sigma$ . The net surface heat flux anomalies in NUDGED are dominated by the latent heat  
279 flux (Fig. 4 e-h). The pattern of surface latent heat flux anomalies in JJA in the extratropical North  
280 Pacific resembles that for the internal PDO structure (Figure 4), with positive flux anomalies  
281 extending eastward from the KOE region, which are enveloped by negative anomalies in the  
282 northeast Pacific and subtropical North Pacific. The positive heat fluxes exhibited in the KOE  
283 region in all seasons outside of DJF are evidence that cold SST anomalies in this region reduce  
284 heat loss to the atmosphere throughout the simulations. Regions such as those in the north-east  
285 North Pacific appear to dampen the SST anomalies during MAM and JJA, which may indicate  
286 limited dynamic feedback to the atmosphere. However, across the central North Pacific, the  
287 persistence of surface latent flux anomalies year-round is expected given the surface temperature  
288 persistence and alludes to ocean-atmosphere feedbacks.

289

### 290 *3.3 Atmospheric circulation response*

291 Figure 5 shows the seasonal mean zonal and meridional near-surface wind anomalies in  
292 NUDGED. As expected, the largest anomalies occur in the period over which nudging is applied  
293 (DJF), with a westerly zonal wind anomaly of up to  $\sim 0.5 \text{ ms}^{-1}/\sigma$  in the subtropics and an easterly  
294 anomaly of a similar magnitude in the subpolar extratropics. The meridional wind shows  
295 alternating southerly-northerly anomalies across the North Pacific orientated with a north-easterly  
296 tilt suggesting that a persistently strong AL invokes a modulation of the climatological Rossby  
297 wave train providing a pathway for atmospheric communication between the North Pacific and  
298 eastern tropical Pacific. Evidence for the modulation of the Rossby wave train is further evident  
299 in the upper tropospheric winds (Figure S5). The subtropical zonal wind anomalies project onto a

300 southerly shift of the westerlies compared to the climatology in CONTROL, with persistent  
301 anomalies extending into the spring after nudging ceases (MAM). Interestingly, there is an  
302 emergence of a westerly wind anomaly near the coast of Central America in DJF that extends  
303 southward and westward into the equatorial Pacific in MAM. Although zonal wind anomalies are  
304 evident in JJA, they are not strongly statistically significant.

305 Figure 6 shows the latitude-time evolution of surface temperature, near-surface wind and surface  
306 pressure anomalies in NUDGED averaged over the central and eastern tropical Pacific. There is  
307 year-round warming in subtropical and equatorial regions, with the largest magnitude in the  
308 subtropics from November through April ( $\sim 0.05$  K/ $\sigma$ ) and in the equatorial region from March  
309 through July ( $\sim 0.3$  K/ $\sigma$ ). The nudging invokes concurrent warming in the subtropics, while there  
310 is a seasonal delay in the emergence of warming in the equatorial Pacific. From July to November  
311 in the subtropics (around  $15^\circ\text{N}$ ) there is substantially less warming than during the rest of the  
312 year, with values close to zero. The westerly wind anomalies coincide with the timing of the  
313 temperature anomalies, with south-westerly anomalies of  $\sim 0.05$  m s $^{-1}$ / $\sigma$  in the subtropics and  
314  $\sim 0.03$  m s $^{-1}$ / $\sigma$  in the equatorial region. In addition to the cross-equatorial temperature gradient  
315 generated by the subtropical anomaly, the lower surface pressure in the northern subtropics ( $\sim 1.5$   
316 hPa), which is largest in February and March, creates a pressure gradient across the equator, a  
317 key component of the WES mechanism. At this time there is evidence of cooling in the southern  
318 subtropics (south of  $15^\circ\text{S}$ ).

319

#### 320 **4. Discussion**

321

322 The impact of an intensified Aleutian Low on the tropical Pacific in this study suggests an  
323 excitation of the SFM mechanism (e.g. Vimont et al. 2003; Alexander et al. 2010; Chen and Yu,  
324 2020; Sun and Okumura, 2019). In accordance with the SFM, the SST anomalies persist into the  
325 summer season, with anomalous temperatures found in the North Pacific year-round. The signals  
326 in winter and spring show a similar spatial signature to that found by Liguori and Di Lorenzo  
327 (2019), who show an SST signature in the subtropics as a precursor to ENSO dynamics. Here  
328 we find a similar effect on multi-year timescales in response to an anomalous Aleutian Low.

329

330 The midlatitude westerly winds show a southerly shift throughout the year which, in agreement  
331 with Liu et al. (2021), acts to prevent heat loss from the surface due to reduced evaporation. This  
332 in turn drives the SST anomaly towards the equator. Liu et al. (2021) show the SFM as the  
333 mechanism that propagates SST anomalies southward, through a change in latent heat fluxes.

334 However, in DJF the westerly winds imposed by the nudging cause a weakening of the subtropical  
335 trades; hence the southerly shift of westerlies starts to occur within the season of nudging. We  
336 show anomalous latent heat flux is responsible for the change in subtropical North Pacific SSTs.  
337 The limitation of the Liu et al. (2021) study is that the atmosphere was coupled to a thermodynamic  
338 slab-ocean, whereas we integrate a fully coupled ocean model allowing for a role of ocean  
339 dynamical feedbacks. Sun and Okumura (2019) conducted a related investigation by imposing  
340 heat flux anomalies associated with the North Pacific Oscillation (NPO), which is a coupled  
341 atmosphere-ocean mode, but they imposed a fixed year round anomaly whereas the Aleutian  
342 Low shows strongest variability in winter and therefore we only impose relaxation during boreal  
343 winter in our experimental design. The simulations presented use an anomalous Aleutian Low  
344 state taken from a single month (Figure S3). An area for future research is to impose a suite of  
345 varying Aleutian Low states with different spatial and temporal profiles to test the sensitivity of the  
346 responses described here to details of the imposed relaxation state.

347  
348 In the tropical Pacific, the dominant mechanism responsible for the increase in SSTs is meridional  
349 advection, with the change to meridional current velocity driving the accelerated warming in boreal  
350 spring. This coincides with a northward cross-equatorial SST gradient and the development of an  
351 anomalous cross-equatorial southward pressure gradient. Cross-equatorial winds are generated,  
352 which, due to Coriolis force act to weaken the trades in the northern equatorial region, decreasing  
353 the surface latent heat flux and leading to a local warming. The heat budget analysis shows that  
354 surface heat fluxes are the primary warming agent during the nudging period, whereas a change  
355 to surface advection drives the warming in the central tropical Pacific. A comprehensive review of  
356 this mechanism, commonly referred to as the wind-evaporation-SST (WES) mechanism, is  
357 provided in Mahajan et al. (2008). Further, the mechanism has been posited as a pathway through  
358 which North Pacific SSTs can influence ENSO variability (Amaya et al. 2019). Investigation into  
359 equatorial thermocline depth shows a slight deepening of the thermocline in all seasons apart  
360 from SON, which is supported by changes in the vertical advection term (not shown). Figure 7  
361 gives a pictorial representation of the combined mechanisms involved in translating the Aleutian  
362 Low anomaly into the deep tropics.

363  
364 While the results make conceptual sense and are in broad agreement with studies using more  
365 comprehensive modelling tools (see earlier references), the amplitude of the response could be  
366 verified in other more detailed coupled climate models. The coarseness of the coupled model,  
367 specifically the vertical dimension of the oceanic component, is a limitation of the study.  
368 Specifically, the model's relatively low resolution and inability to resolve mesoscale processes in

369 the ocean and atmosphere may affect the results of the study. Future studies using observations  
370 and higher resolution GCMs to test the results herein would be valuable. Furthermore, to ensure  
371 model stability, the anomalous nudging state was drawn from the coupled atmosphere-ocean  
372 control simulation. The Aleutian Low variability sampled from this simulation therefore includes  
373 effects from tropical variability. The month used as the reference state for the nudging coincides  
374 with an ENSO state (magnitude = 0.55) in the tropical Pacific. Further study could investigate  
375 more idealised AL states and their effects on extra-tropical-tropical communication.

376

## 377 **5. Conclusions**

378

379 Externally-forced Aleutian Low trends have been implicated as a potential driver of recent  
380 variations in the Pacific Decadal Oscillation (Smith et al., 2016; Klavans et al., submitted). Here,  
381 we have investigated the potential influence of Aleutian Low trends on basin-wide low frequency  
382 Pacific sea surface temperature variability using nudging simulations in an intermediate  
383 complexity climate model. The target Aleutian Low state represents an extremely intense Aleutian  
384 Low state ( $-3\sigma$  of winter monthly variability) applied during boreal winter. The intensified Aleutian  
385 Low induces a basin-wide SST response that resembles the model's internally-generated PDO  
386 with a comparable amplitude in the extratropics, but a substantially weaker amplitude in the  
387 equatorial Pacific by a factor of 4 to 5. The pattern of SST variability exhibited across the basin is  
388 evident on interannual timescales as well as throughout the duration of the 30 year simulation.

389

390 The findings presented here support that the PDO can, at least in part, be driven by remotely  
391 forced changes in the North Pacific atmospheric circulation independent of the tropics. However,  
392 in our experiment the amplitude appears to be too weak to fully explain a multi-annual shift in the  
393 PDO across the tropics. This suggests that the hypothesis posed by Smith et al. (2016) and  
394 Klavans et al. (submitted), that anthropogenically forced changes in the Aleutian Low drove the  
395 observed shift in the phase of the basin-wide PDO in the late 20th and early 21st centuries, should  
396 be revisited.

397

### 398 **Code availability**

399

400 The nudging code used in the analysis can be found:  
401 (<https://github.com/NOC-MSM/FORTE2.0>).

402

### 403 **Data availability**

404

405 Underlying model data found in this paper is available from the corresponding author upon  
406 request.

407

408 HadISST data available: <https://www.metoffice.gov.uk/hadobs/hadisst/data/download.html>

409

#### 410 **Author contribution**

411

412 WJD and ACM designed the study. WJD developed the nudging code in FORTE2.0 with support  
413 from CMM, MMJ and RR. ATB and RR helped with installation of FORTE2.0 at Leeds. WJD  
414 performed the analysis and produced the figures. WJD and ACM wrote the manuscript with  
415 comments from all authors. All simulations were performed on the ARC4 HPC at the University  
416 of Leeds.

417

#### 418 **Competing interests**

419

420 The authors declare that they have no conflict of interest.

421

#### 422 **Acknowledgements**

423

424 WJD was supported by a Natural Environment Research Council (NERC) Ph.D. studentship  
425 through the SPHERES Doctoral Training Partnership (NE/L002574/1) and by a Met Office CASE  
426 studentship. ACM and CMM were supported by the European Union's Horizon 2020 Research  
427 and Innovation Programme under Grant Agreement 820829 (CONSTRAIN project). ACM was  
428 supported by the Leverhulme Trust. We are grateful to Paloma Trascasa-Castro for discussion of  
429 ENSO processes. We are grateful for feedback on an earlier version of this manuscript from John  
430 Marsham and Laura Wilcox.

431

#### 432 **References**

433

434 Alexander, M. A., & Deser, C. (1995). A mechanism for the recurrence of wintertime  
435 midlatitude SST anomalies. *Journal of Physical Oceanography*, 25(1), 122–137.  
436 [https://doi.org/10.1175/1520-0485\(1995\)025<0122:AMFTRO>2.0.CO;2](https://doi.org/10.1175/1520-0485(1995)025<0122:AMFTRO>2.0.CO;2)

437 Alexander, M. A., Vimont, D. J., Chang, P., & Scott, J. D. (2010). The impact of  
438 extratropical atmospheric variability on ENSO: Testing the seasonal footprinting  
439 mechanism using coupled model experiments. *Journal of Climate*, 23(11), 2885–  
440 2901. <https://doi.org/10.1175/2010JCLI3205.1>

441 Amaya, D. J., Kosaka, Y., Zhou, W., Zhang, Y., Xie, S. P., & Miller, A. J. (2019). The North  
442 Pacific pacemaker effect on historical ENSO and its mechanisms. *Journal of Climate*,  
443 32(22), 7643–7661. <https://doi.org/10.1175/JCLI-D-19-0040.1>

444 Barnett, T. P., Pierce, D. W., & Planck, M. (1999). Interdecadal interactions between the  
445 tropics and midlatitudes in the Pacific basin. *Geophysical Research Letters*, 26(5),  
446 615–618.

447 Blaker, A., Joshi, M., Sinha, B., Stevens, D., Smith, R., & Hirschi, J. (2021). FORTE 2.0: a  
448 fast, parallel and flexible coupled climate model. *Geoscientific Model Development*,  
449 275–293. <https://doi.org/10.5194/gmd-14-275-2021>

450 Chen, S., & Yu, B. (2020). The seasonal footprinting mechanism in large ensemble  
451 simulations of the second generation Canadian earth system model: uncertainty due  
452 to internal climate variability. *Climate Dynamics*, 55(9–10), 2523–2541.  
453 <https://doi.org/10.1007/s00382-020-05396-y>

454 Clement, A., DiNezio, P., & Deser, C. (2011). Rethinking the ocean’s role in the Southern  
455 Oscillation. *Journal of Climate*, 24(15), 4056–4072.  
456 <https://doi.org/10.1175/2011JCLI3973.1>

457 Czaja, A., van der Vaart, P., & Marshall, J. (2002). A diagnostic study of the role of remote  
458 forcing in tropical Atlantic variability. *Journal of Climate*, 15(22), 3280–3290.  
459 [https://doi.org/10.1175/1520-0442\(2002\)015<3280:ADSOTR>2.0.CO;2](https://doi.org/10.1175/1520-0442(2002)015<3280:ADSOTR>2.0.CO;2)

460 Deser, C., Sun, L., Tomas, R. A., & Screen, J. (2016). Does ocean coupling matter for the  
461 northern extratropical response to projected Arctic sea ice loss? *Geophysical  
462 Research Letters*, 43(5), 2149–2157. <https://doi.org/10.1002/2016GL067792>

463 Dittus, A. J., Hawkins, E., Robson, J. I., Smith, D. M., & Wilcox, L. J. (2021). Drivers of  
464 Recent North Pacific Decadal Variability: The Role of Aerosol Forcing. *Earth’s Future*,  
465 9(12). <https://doi.org/10.1029/2021EF002249>

466 Dow, W. J., Maycock, A. C., Lofverstrom, M., & Smith, C. J. (2021). The effect of  
467 anthropogenic aerosols on the aleutian low. *Journal of Climate*, 34(5), 1725–1741.  
468 <https://doi.org/10.1175/JCLI-D-20-0423.1>

469 Gan, B. L. Wu, F Jia, S. Li, W. Cai, H. Nakamura, M. A. Alexander, and A. J. Miller,  
470 2017: On the response of the Aleutian Low to greenhouse warming. *J. Climate*,  
471 30, 3907-3925, doi: 10.1175/JCLI-D-15-0789.1

472 Gu, D., & Philander, S. G. H. (1997). Interdecadal climate fluctuations that depend on  
473 exchanges between the tropics and extratropics. *Science*, 275(5301), 805–807.  
474 <https://doi.org/10.1126/science.275.5301.805>

475 Hu, D., & Guan, Z. (2018). Decadal relationship between the stratospheric arctic vortex and  
476 pacific decadal oscillation. *Journal of Climate*, 31(9), 3371–3386.  
477 <https://doi.org/10.1175/JCLI-D-17-0266.1>

478 Jin, F. F. (2001). Low-frequency modes of tropical ocean dynamics. *Journal of Climate*,  
479 14(18), 3874–3881. [https://doi.org/10.1175/1520-  
480 0442\(2001\)014<3874:LFMOTO>2.0.CO;2](https://doi.org/10.1175/1520-0442(2001)014<3874:LFMOTO>2.0.CO;2)

481 Joshi, M., Hall, R. A., Stevens, D. P., and Hawkins, E.: The modelled climatic response  
482 to the 18.6-year lunar nodal cycle and its role in decadal temperature trends, *Earth*  
483 *Syst. Dynam.*, 14, 443–455, <https://doi.org/10.5194/esd-14-443-2023>, 2023.

484 Joshi, M., Stringer, M., Van Der Wiel, K., O’Callaghan, A., & Fueglistaler, S. (2015).  
485 IGCM4: A fast, parallel and flexible intermediate climate model. *Geoscientific Model*  
486 *Development*, 8(4), 1157–1167. <https://doi.org/10.5194/gmd-8-1157-2015>

487 Klavans et al. (2023) Recent Atlantic multidecadal variability and its impacts are driven by  
488 external forcings, submitted

489 Knight, J. R., Maidens, A., Watson, P. A. G., Andrews, M., Belcher, S., Brunet, G.,  
490 Fereday, D., Folland, C. K., Scaife, A. A., & Slingo, J. (2017). Global meteorological  
491 influences on the record UK rainfall of winter 2013-14. *Environmental Research*  
492 *Letters*, 12(7). <https://doi.org/10.1088/1748-9326/aa693c>



- 493 Knutson, T. R., & Manabe, S. (1998). Model assessment of decadal variability and trends  
494 in the tropical Pacific Ocean. In *Journal of Climate* (Vol. 11, Issue 9).  
495 [https://doi.org/10.1175/1520-0442\(1998\)011<2273:MAODVA>2.0.CO;2](https://doi.org/10.1175/1520-0442(1998)011<2273:MAODVA>2.0.CO;2)
- 496 Kwon, Y. O., & Deser, C. (2007). North Pacific decadal variability in the community climate  
497 system model version 2. *Journal of Climate*, 20(11), 2416–2433.  
498 <https://doi.org/10.1175/JCLI4103.1>
- 499 Latif, M., & Barnett, T. P. (1996). Decadal climate variability over the North Pacific and  
500 North America: Dynamics and predictability. *Journal of Climate*, 9(10), 2407–2423.  
501 [https://doi.org/10.1175/1520-0442\(1996\)009<2407:DCVOTN>2.0.CO;2](https://doi.org/10.1175/1520-0442(1996)009<2407:DCVOTN>2.0.CO;2)
- 502 Liguori, G., & Di Lorenzo, E. (2019). Separating the North and South Pacific Meridional  
503 Modes Contributions to ENSO and Tropical Decadal Variability. *Geophysical*  
504 *Research Letters*, 46(2), 906–915. <https://doi.org/10.1029/2018GL080320>
- 505 Litzow, M. A., Malick, M. J., Bond, N. A., Cunningham, C. J., Gosselin, J. L., & Ward, E. J.  
506 (2020). Quantifying a Novel Climate Through Changes in PDO-Climate and PDO-  
507 Salmon Relationships. *Geophysical Research Letters*, 47(16), e2020GL087972.  
508 <https://doi.org/10.1029/2020GL087972>
- 509 Liu, Y., Sun, C., Kucharski, F., Li, J., Wang, C., & Ding, R. (2021). The North Pacific Blob  
510 acts to increase the predictability of the Atlantic warm pool. *Environmental Research*  
511 *Letters*, 16(6), 064034. <https://doi.org/10.1088/1748-9326/ac0030>
- 512 Lysne, J. A., Chang, P., & Giese, B. (1997). Impact of the extratropical Pacific on equatorial  
513 variability. *Geophysical Research Letters*, 24(21), 2589–2592.  
514 <https://doi.org/10.1029/97GL02751>
- 515 Mantua, N. J., Hare, S. R., Zhang, Y., Wallace, J. M., & Francis, R. C. (1997). A Pacific  
516 Interdecadal Climate Oscillation with Impacts on Salmon Production. *Bulletin of the*  
517 *American Meteorological Society*, 78(6), 1069–1079. [https://doi.org/10.1175/1520-0477\(1997\)078<1069:APICOW>2.0.CO;2](https://doi.org/10.1175/1520-0477(1997)078<1069:APICOW>2.0.CO;2)
- 518
- 519 Mahajan, S., Saravanan, R., & Chang, P. (2009). The role of the wind-evaporation-sea  
520 surface temperature (WES) feedback in air-sea coupled tropical variability.  
521 *Atmospheric Research*, 94(1), 19–36. <https://doi.org/10.1016/j.atmosres.2008.09.017>

- 522 Martin, Z., Orbe, C., Wang, S., & Sobel, A. (2021). The MJO–QBO relationship in a GCM  
523 with stratospheric nudging. *Journal of Climate*, 34(11), 4603–4624.  
524 <https://doi.org/10.1175/JCLI-D-20-0636.1>
- 525 McCreary, J. P., & Peng Lu. (1994). Interaction between the subtropical and equatorial  
526 ocean circulations: the subtropical cell. *Journal of Physical Oceanography*, 24(2),  
527 466–497. [https://doi.org/10.1175/1520-0485\(1994\)024<0466:IBTSAE>2.0.CO;2](https://doi.org/10.1175/1520-0485(1994)024<0466:IBTSAE>2.0.CO;2)
- 528 Nagano, A., & Wakita, M. (2019). Wind-driven decadal sea surface height and main  
529 pycnocline depth changes in the western subarctic North Pacific. *Progress in Earth  
530 and Planetary Science*, 6(1), 1–26. <https://doi.org/10.1186/s40645-019-0303-0>
- 531 Newman, M., Alexander, M. A., Ault, T. R., Cobb, K. M., Deser, C., Di Lorenzo, E., Mantua,  
532 N. J., Miller, A. J., Minobe, S., Nakamura, H., Schneider, N., Vimont, D. J., Phillips, A.  
533 S., Scott, J. D., & Smith, C. A. (2016). The Pacific decadal oscillation, revisited.  
534 *Journal of Climate*, 29(12), 4399–4427. <https://doi.org/10.1175/JCLI-D-15-0508.1>
- 535 Pickart, R. S., Moore, G. W. K., Macdonald, A. M., Renfrew, I. A., Walsh, J. E., & Kessler,  
536 W. S. (2009). Seasonal evolution of Aleutian low pressure systems: Implications for  
537 the North Pacific subpolar circulation. *Journal of Physical Oceanography*, 39(6),  
538 1317–1339. <https://doi.org/10.1175/2008JPO3891.1>
- 539 Pierce, D. W., Barnett, T. P., & Latif, M. (2000). Connections between the Pacific Ocean  
540 Tropics and midlatitudes on decadal timescales. *Journal of Climate*, 13(6), 1173–  
541 1194. [https://doi.org/10.1175/1520-0442\(2000\)013<1173:CBTPOT>2.0.CO;2](https://doi.org/10.1175/1520-0442(2000)013<1173:CBTPOT>2.0.CO;2)
- 542 Richter, J. H., Deser, C., & Sun, L. (2015). Effects of stratospheric variability on El Niñ.  
543 *Environmental Research Letters*, 10(12). [https://doi.org/10.1088/1748-  
544 9326/10/12/124021](https://doi.org/10.1088/1748-9326/10/12/124021)
- 545 Schneider, N., & Cornuelle, B. D. (2005). The forcing of the Pacific Decadal Oscillation.  
546 *Journal of Climate*, 18(21), 4355–4373. <https://doi.org/10.1175/JCLI3527.1>
- 547 Schneider, N., Miller, A. J., & Pierce, D. W. (2002). Anatomy of North Pacific decadal  
548 variability. In *Journal of Climate* (Vol. 15, Issue 6). [https://doi.org/10.1175/1520-  
549 0442\(2002\)015<0586:AONPDV>2.0.CO;2](https://doi.org/10.1175/1520-0442(2002)015<0586:AONPDV>2.0.CO;2)

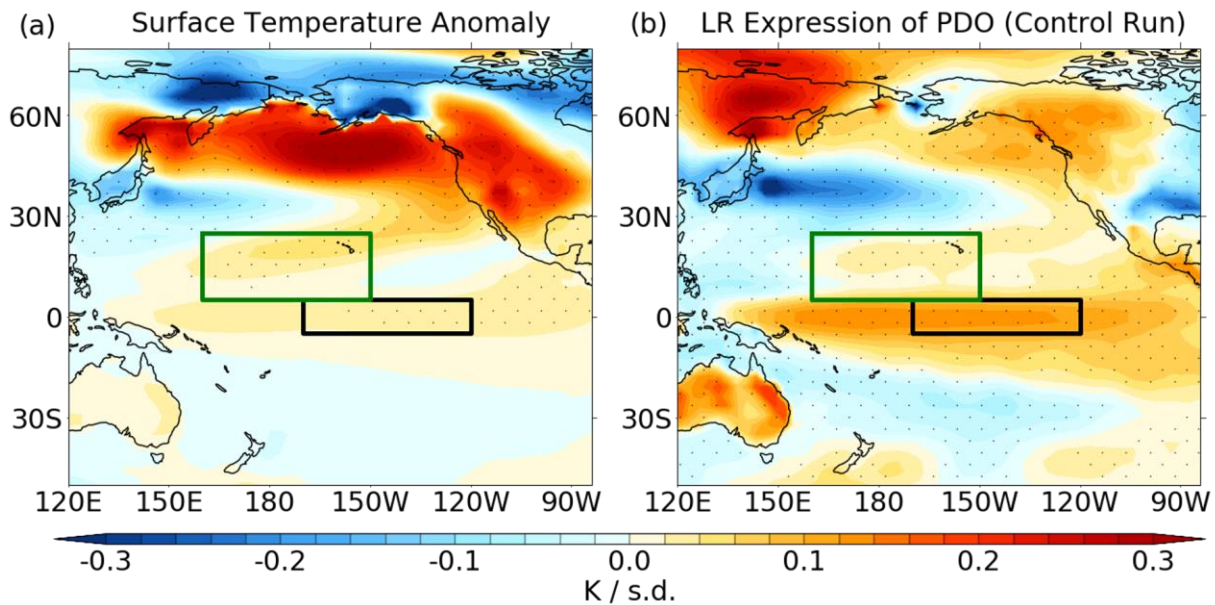
- 550 Simon, A., Gastineau, G., Frankignoul, C., Rousset, C., & Codron, F. (2021). Transient  
551 climate response to Arctic Sea ice loss with two ice-constraining methods. *Journal of*  
552 *Climate*, 34(9), 3295–3310. <https://doi.org/10.1175/JCLI-D-20-0288.1>
- 553 Smith, D. M., Booth, B. B. B., Dunstone, N. J., Eade, R., Hermanson, L., Jones, G. S.,  
554 Scaife, A. A., Sheen, K. L., & Thompson, V. (2016). Role of volcanic and  
555 anthropogenic aerosols in the recent global surface warming slowdown. *Nature*  
556 *Climate Change*, 6(10), 936–940. <https://doi.org/10.1038/nclimate3058>
- 557 Sugimoto, S., & Hanawa, K. (2009). Decadal and interdecadal variations of the Aleutian  
558 Low activity and their relation to upper oceanic variations over the North Pacific.  
559 *Journal of the Meteorological Society of Japan*, 87(4), 601–614.  
560 <https://doi.org/10.2151/jmsj.87.601>
- 561 Sun, J., & Wang, H. (2006). Relationship between Arctic Oscillation and Pacific Decadal  
562 Oscillation on decadal timescale. *Chinese Science Bulletin*, 51(1), 75–79.  
563 <https://doi.org/10.1007/s11434-004-0221-3>
- 564 Sun, T., & Okumura, Y. M. (2019). Role of stochastic atmospheric forcing from the south  
565 and North Pacific in tropical Pacific decadal variability. *Journal of Climate*, 32(13),  
566 4013–4038. <https://doi.org/10.1175/JCLI-D-18-0536.1>
- 567 Taguchi, B., Xie, S. P., Schneider, N., Nonaka, M., Sasaki, H., & Sasai, Y. (2007). Decadal  
568 variability of the Kuroshio Extension: Observations and an eddy-resolving model  
569 hindcast. *Journal of Climate*, 20(11), 2357–2377. <https://doi.org/10.1175/JCLI4142.1>
- 570 Trenberth, K. E., & Hurrell, J. W. (1994). Decadal atmosphere-ocean variations in the  
571 Pacific. *Climate Dynamics*, 9(6), 303–319. <https://doi.org/10.1007/BF00204745>
- 572 Vimont, D. J. (2005). The contribution of the interannual ENSO cycle to the spatial pattern  
573 of decadal ENSO-like variability. In *Journal of Climate* (Vol. 18, Issue 12).  
574 <https://doi.org/10.1175/JCLI3365.1>
- 575 Vimont, D. J., Battisti, D. S., & Hirst, A. C. (2001). Footprinting: A seasonal connection  
576 between the tropics and mid-latitudes. *Geophysical Research Letters*, 28(20), 3923–  
577 3926. <https://doi.org/10.1029/2001GL013435>

- 578 Vimont, D. J., Battisti, D. S., & Hirst, A. C. (2002). Pacific interannual and interdecadal  
579 equatorial variability in a 1000-Yr simulation of the CSIRO coupled general circulation  
580 model. *Journal of Climate*, *15*(2), 160–178. [https://doi.org/10.1175/1520-](https://doi.org/10.1175/1520-0442(2002)015<0160:PIAIEV>2.0.CO;2)  
581 [0442\(2002\)015<0160:PIAIEV>2.0.CO;2](https://doi.org/10.1175/1520-0442(2002)015<0160:PIAIEV>2.0.CO;2)
- 582 Vimont, D. J., Wallace, J. M., & Battisti, D. S. (2003). The seasonal footprinting mechanism  
583 in the Pacific: Implications for ENSO. *Journal of Climate*, *16*(16), 2668–2675.  
584 [https://doi.org/10.1175/1520-0442\(2003\)016<2668:TSFMIT>2.0.CO;2](https://doi.org/10.1175/1520-0442(2003)016<2668:TSFMIT>2.0.CO;2)
- 585 Wang, H., Kumar, A., Wang, W., & Xue, Y. (2012). Seasonality of the Pacific decadal  
586 oscillation. *Journal of Climate*, *25*(1), 25–38. <https://doi.org/10.1175/2011JCLI4092.1>
- 587 Watson, P. A. G., Weisheimer, A., Knight, J. R., & Palmer, T. N. (2016). The role of the  
588 tropical West Pacific in the extreme Northern Hemisphere winter of 2013/2014.  
589 *Journal of Geophysical Research*, *121*(4), 1698–1714.  
590 <https://doi.org/10.1002/2015JD024048>
- 591 Webb, D. J. (1996). An ocean model code for array processor computers. *Computers and*  
592 *Geosciences*, *22*(5), 569–578. [https://doi.org/10.1016/0098-3004\(95\)00133-6](https://doi.org/10.1016/0098-3004(95)00133-6)
- 593 Wills, R. C. J., Battisti, D. S., Proistosescu, C., Thompson, L. A., Hartmann, D. L., &  
594 Armour, K. C. (2019). Ocean Circulation Signatures of North Pacific Decadal  
595 Variability. *Geophysical Research Letters*, *46*(3), 1690–1701.  
596 <https://doi.org/10.1029/2018GL080716>
- 597 Xie, S. P., & Tanimoto, Y. (1998). A pan-Atlantic decadal climate oscillation. *Geophysical*  
598 *Research Letters*, *25*(12), 2185–2188. <https://doi.org/10.1029/98GL01525>
- 599 Zhang, D., & McPhaden, M. J. (2006). Decadal variability of the shallow Pacific meridional  
600 overturning circulation: Relation to tropical sea surface temperatures in observations  
601 and climate change models. *Ocean Modelling*, *15*(3–4), 250–273.  
602 <https://doi.org/10.1016/j.ocemod.2005.12.005>
- 603 Zhang, Y., Xie, S. P., Kosaka, Y., & Yang, J. C. (2018). Pacific decadal oscillation: Tropical  
604 Pacific forcing versus internal variability. *Journal of Climate*, *31*(20), 8265–8279.  
605 <https://doi.org/10.1175/JCLI-D-18-0164.1>

606 Zhao, Y., Newman, M., Capotondi, A., Lorenzo, E. Di, & Sun, D. (2021). Removing the  
607 effects of tropical dynamics from north pacific climate variability. *Journal of Climate*,  
608 34(23), 9249–9265. <https://doi.org/10.1175/JCLI-D-21-0344.1>

609  
610  
611  
612  
613  
614  
615  
616  
617  
618  
619  
620  
621  
622  
623  
624

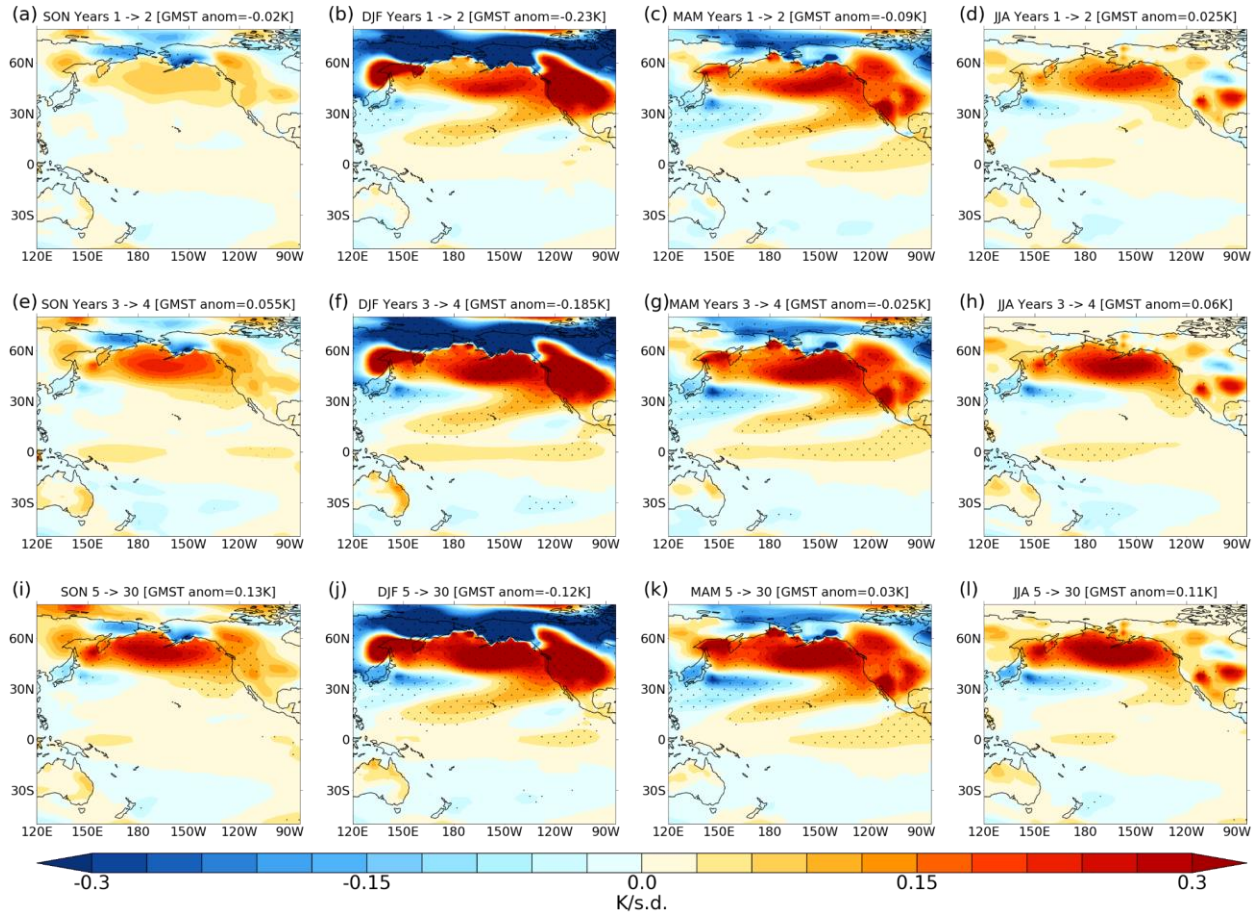
**Figures**



625  
626 **Figure 1:** Annual mean surface temperature anomalies for (a) ensemble mean anomaly  
627 in NUDGED averaged over years 1-30; (b) regression onto the PDO index in CONTROL.

628 Units are K per standard deviation. Stippling denotes anomalies that are significant at the  
 629 95% level. Green and black boxes show the regions for the mixed layer heat budget  
 630 analysis.

631



632

633

634 **Figure 2:** Seasonal mean surface temperature anomalies in NUDGED expressed per  
 635 unit PDO index [K/σ] for SON, DJF, MAM and JJA. Composite anomalies are shown for  
 636 years 1-2 (a-d), years 3-4 (e-h) and years 5-30 (i-l). Global mean surface temperature  
 637 anomalies are shown in the header. Stippling denotes anomalies that are significant at  
 638 the 95% level.

639

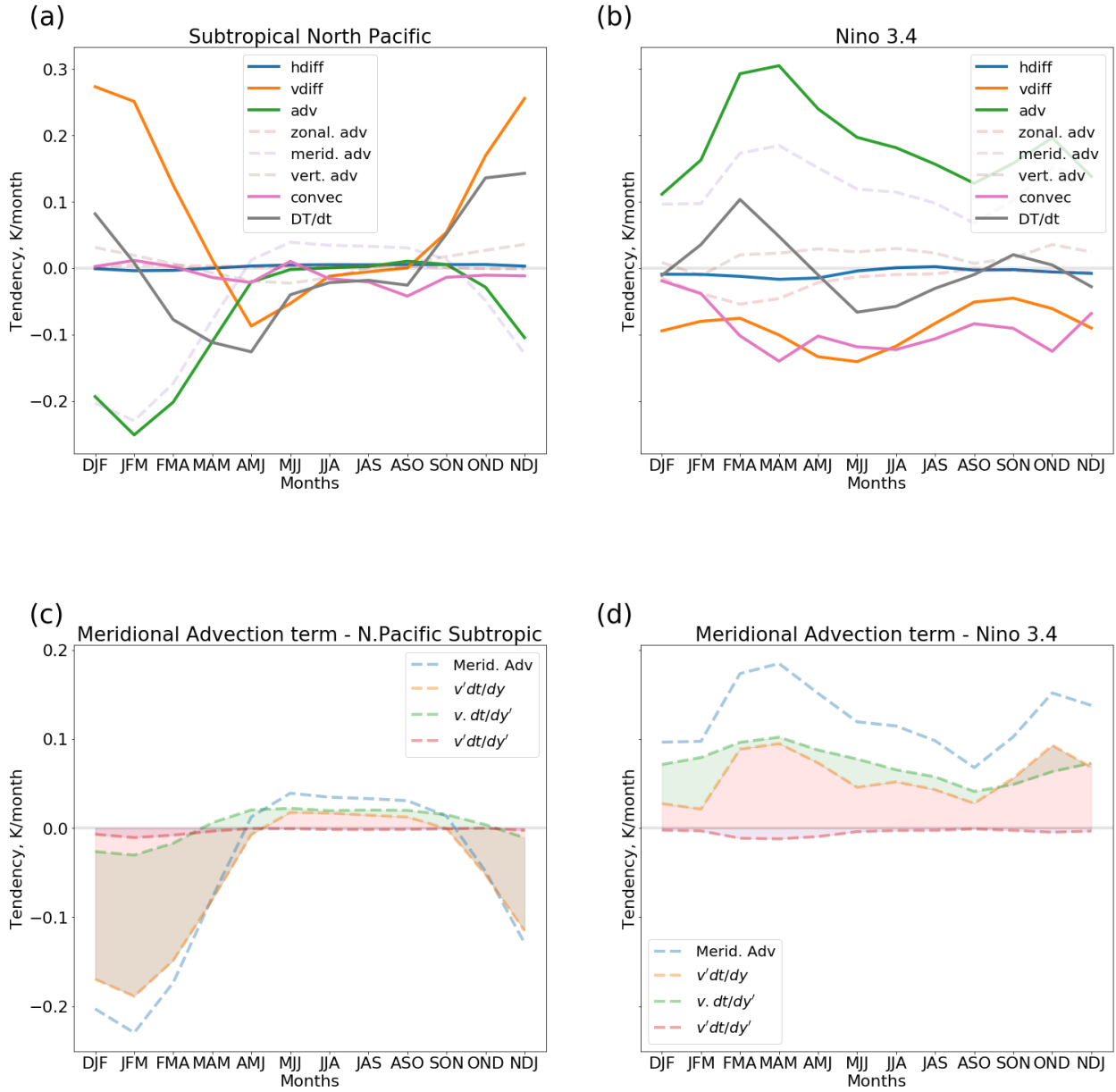
640

641

642

643

644  
645  
646  
647

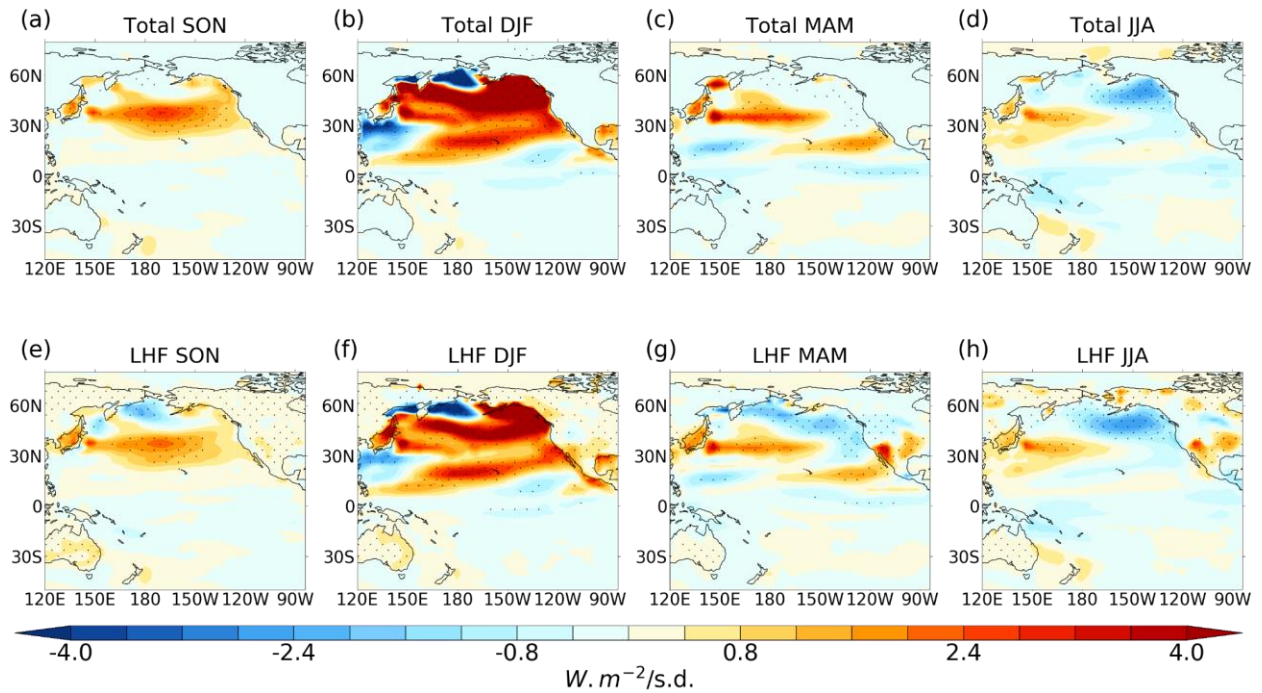


648  
649  
650

651  
652

653 **Figure 3:** Years 1-30, 3-month moving average of anomalous NUDGED-CONTROL  
654 mixed layer temperature tendencies and constituent heat budget terms for the (a)  
655 subtropical North Pacific and (b) Niño 3.4 regions. (c,d) show the meridional advection  
656 term and its linear expansion.

657



658

659

660

661

662

663

664

665

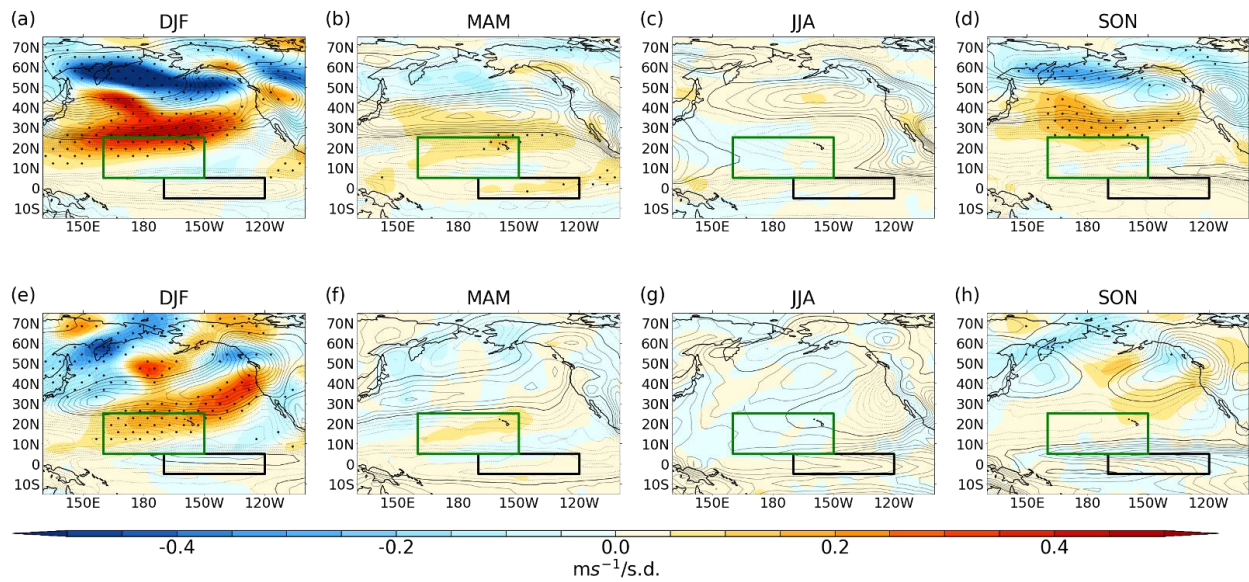
666

667

668

**Figure 4:** (a-d) Years 1-30 seasonal mean net surface heat flux anomalies in NUDGED. (e-h): Years 1-30 seasonal mean latent heat flux anomaly in NUDGED. Positive denotes downward flux. Stippling denotes anomalies that are statistically significant at the 95% level. Units:  $W \cdot m^{-2}$  per standard deviation.

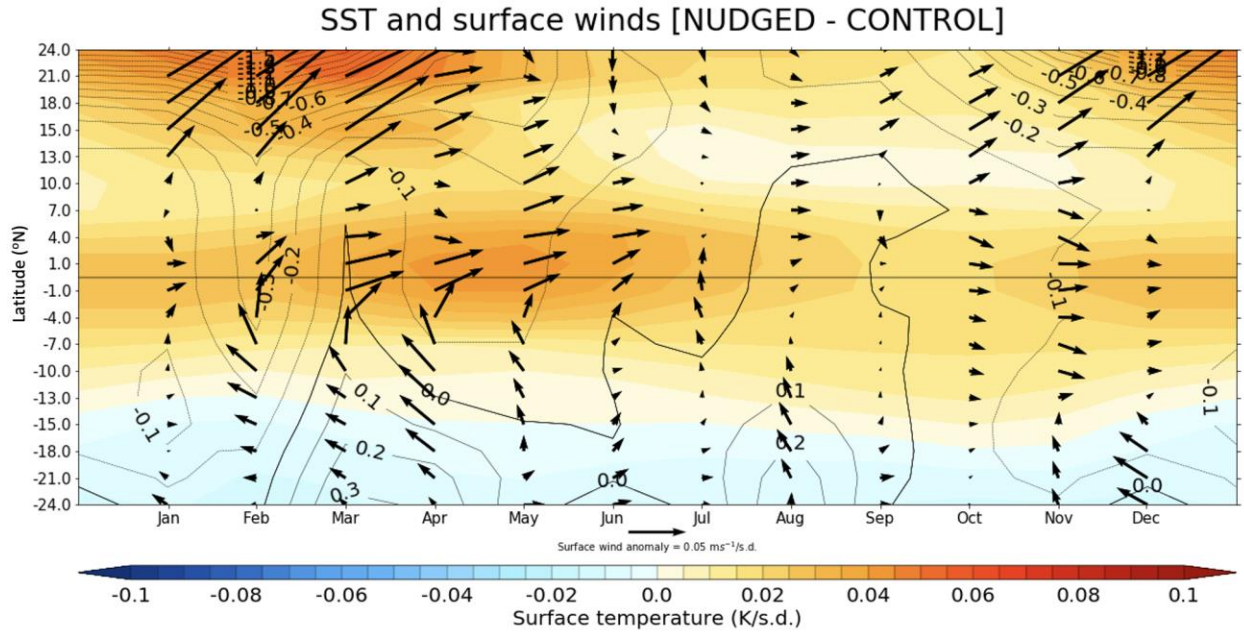




669  
670

671 **Figure 5:** Years 1-30 seasonal mean NUDGED-CONTROL near-surface wind anomalies  
 672 for (a-d) zonal and (e-h) meridional wind. Contours show climatology of CONTROL  
 673 (dashed lines are negative values, contour interval  $1 \text{ m s}^{-1}$ ). Stippling denotes anomalies  
 674 that are significant at the 95% level.

675  
676  
677  
678  
679  
680



681

682

683 **Figure 6:** Years 1-30 latitude-time section of NUDGED-CONTROL SST anomaly (K/ $\sigma$ :  
 684 shading), surface pressure (hPa/ $\sigma$ : contours) and near-surface wind anomaly (m s<sup>-1</sup>/ $\sigma$ :  
 685 vectors) averaged over the central-eastern tropical Pacific (205°W-80°W).

686

687

688

689

690

691

692

693

694

695

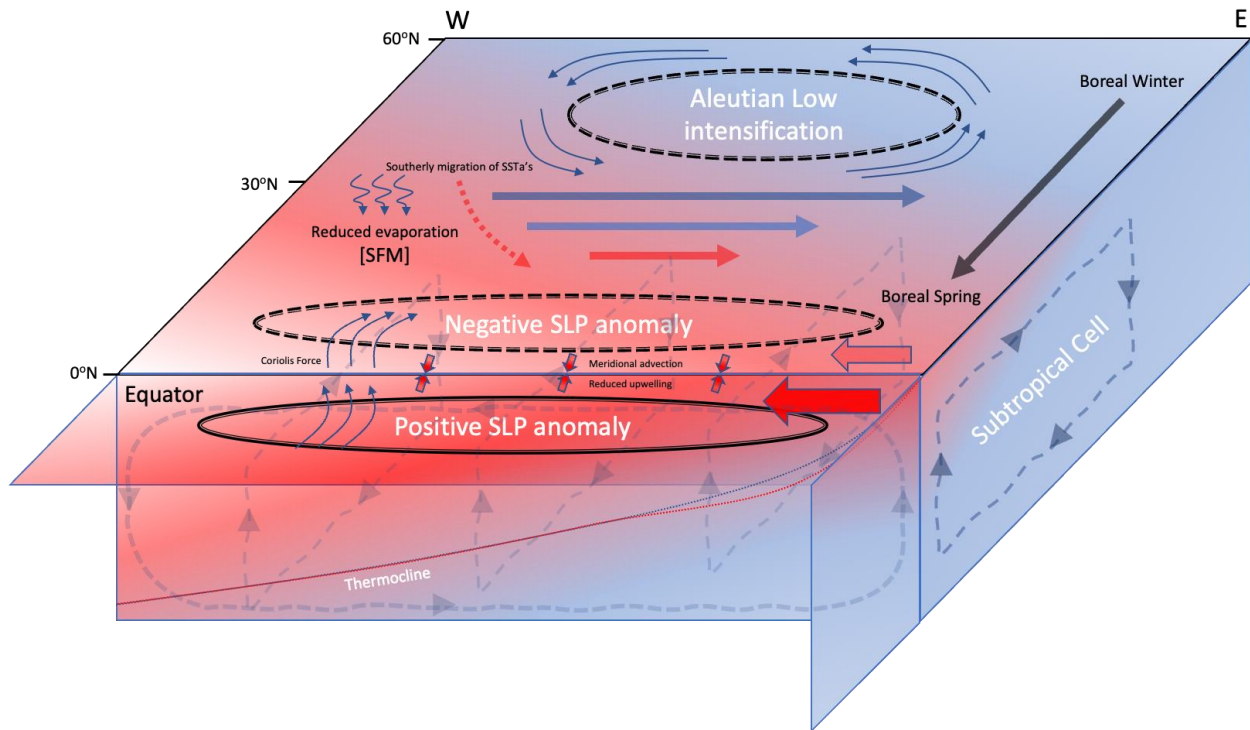
696

697

698

699

700



701  
 702 **Figure 7:** Schematic depicting the mechanisms involved in the tropical SST anomalies  
 703 manifest as a result from an intensification of the AL. An intensified AL (dashed black  
 704 line) imposed during boreal winter is associated with intensified westerlies (solid arrows)  
 705 in the extra-tropics and downward latent heat transfer. The migration of the SST  
 706 anomalies southward during boreal winter is associated with a southerly shift in the  
 707 westerly anomalies. The westerly anomalies act to weaken the background trades (filled  
 708 red arrows) which reduce latent heating due to evaporation and hence an increase in  
 709 extra-tropical Pacific SSTs. In the season after nudging, the temperature asymmetry  
 710 either side of the equator induces an SLP gradient (solid line – positive SLP; dashed  
 711 line – negative SLP) that drives southerly winds across the equator. The Coriolis force  
 712 acts to turn the southerly winds in the southern hemisphere westward and in the  
 713 northern hemisphere eastward. When these anomalous winds are imposed on the  
 714 background easterly trade winds (filled red arrows), the southerlies south of the equator  
 715 increase the wind speed and therefore evaporative cooling, whilst north of the equator  
 716 the background trades are weakened, reducing evaporative cooling. The changes to the  
 717 wind driven surface state act to deepen the thermocline in the eastern tropical Pacific  
 718 (red dotted line) and reduce upwelling/divergence of cooler waters at the equator.  
 719

720  
721  
722